23 European Conference on Fracture – ECF23

Oxidation-Induced Damage Modeling in Micro Gas-Turbine Combustion Chambers

Daniele Cirigliano[a,*], Felix Grimm[a], Peter Kutne[a], Manfred Aigner[a]

[a]*German Aerospace Center (DLR), Pfaffenwaldring 38-40, 70569 Stuttgart, Germany*

Abstract

Combustion chambers of micro gas-turbines are generally operated under very lean global air-fuel ratios for two main reasons: to constrain the production of pollutants (NOx), and to cool-down the metal walls with cooling air. The abundancy of oxygen contained in the air flowing over metal surfaces, together with high temperatures due to combustion, constitute an oxidizing environment. The thin oxide layer can crack due to alternating system operative conditions, potentially initiating a crack detrimental to the combustion chamber's life. An oxidation damage term should be computed in order to provide information of the component's life. In this paper, an oxidation-induced damage model for superalloy INCONEL 718 is applied to a combustion chamber fitting the MTT Enertwin micro gas-turbine. Oxidation growth and material parameters are obtained from experimental data. The phasing of thermal loads with mechanical strains is also considered. The results show a distribution of the oxidation-induced damage on the combustion chamber walls which depend on temperature and mechanical strain rate, suggesting that this damage mechanism is relevant under the given operation conditions. Therefore, the approach should be incorporated in a broader life-assessment methodology, which includes oxidation, creep and potentially mechanical fatigue.

Keywords: Thermomechanical-Fatigue; Oxidation; Creep; Damage; MGT; CFD; FEM.

1. Introduction

Combustion chambers of Micro Gas Turbines (MGT) are subjected to severe thermal loads due to the high temperatures of exhaust gases. The numerous geometrical non-linearities, as well as the different expansion coefficients between materials at junctures, generate mechanical stresses which add to the naturally imposed mechanical load (pressure difference across the walls). Such loads vary during operation in a cyclic manner. At these severe conditions, combustion chambers are prone to crack initiation, which can potentially led to failure. Generally, failure due to the contribution of both thermal and mechanical loading is termed Thermo-Mechanical Fatigue (TMF) (Harrison et al., 1996). TMF conditions produce significant damage contributions from creep, low cycle fatigue and oxidation

---

* Corresponding author. Tel.: +49 711 6862 225.
  E-mail address: daniele.cirigliano@dlr.de

mechanism (Abu et al., 2014). Each of these damage mechanisms have a major or minor impact over the others, depending on the thermal load and mechanical load phasing.

In this analysis, a well-known TMF model is implemented in the Finite Element Method (FEM) software Ansys Mechanical and applied to a MGT combustion chamber, in order to perform a preliminary numerical lifing of the component. In the next section, an overview on the TMF model is outlined. The Computational Fluid Dynamics (CFD) simuations needed to provide the temperature profile on the component are described in a following section. Finally, results for a typical simplified load history are shown.

2. Thermo-mechanical fatigue – numerical models

2.1. The Neu-Sehitoglu TMF damage model

The Neu-Sehitoglu model is one of the most comprehensive damage models for metals, since it considers fatigue, oxidation and creep damage to predict the component's life (Neu and Sehitoglu, 1989a),(Neu and Sehitoglu, 1989b),(Sehitoglu and Boismier, 1990). The damage induced in the material is dictated by the mechanical strain range, strain rate, temperature and the phasing between the temperature and mechanical strain. The total damage per cycle, D_{tot}, is calculated from the sum of fatigue, creep and oxidation damage:

$$D^{tot} = D^{fat} + D^{creep} + D^{ox}. \tag{1}$$

Whereas creep is attributable to long periods of sustained static stress, fatigue is attributable to cyclic mechanical stresses. Since in a MGT's operation there are no mechanical forces applied, the only contribution to fatigue is the pressure difference over the combustion chamber walls due to the slightly different pressure over the liner. This pressure difference is the order of 10^{-3} MPa and is therefore negligible compared to the other terms. For this reason, the only terms included in this analysis are creep and oxidation. Using the Palmgren–Miner linear damage hypothesis (Miner, 1945), a damage fraction, D, is defined as the fraction of life to failure, N_f, used up by an event. Hence, $D = 1/N_f$ and Eq. 1 can be rewritten as:

$$\frac{1}{N_f^{tot}} = \frac{1}{N_f^{creep}} + \frac{1}{N_f^{ox}}. \tag{2}$$

2.2. Creep damage term

The creep damage evolution can be given for example by the modified Lemaitre-Chaboche model (Lemaitre, 1985):

$$\frac{1}{\dot{N}_f^{creep}} = \dot{D}^{creep} = \left(\frac{\sigma_{eq}}{A}\right)^r (1 - D^{creep})^{-k}, \tag{3}$$

where σ_{eq} is the equivalent (Von-Mises) stress and D^{creep} is the scalar creep damage parameter. The creep rupture curve is idealized as a straight line in log-log stress-strain space. Parameter A represents the intercept of the curve with the stress axis, while the exponent r represents the slope; k is used to describe the non-linear damage evolution as observed from damage measurements (Halfpenny et al., 2015). The parameter k is a function of equivalent stress:

$$k = a_0 + a_1(\sigma_{eq} - z) + a_2(\sigma_{eq} - z)^2, \tag{4}$$

where a_0, a_1, a_2, z, r and A are material constants determined by creep tests (see for example (Zhang, 1995)).

2.3. Environmental damage

The environmental term describes the oxidation of metal surfaces in air and relies on measurements of oxide thickness. This term models the environmentally induced crack nucleation and growth due to oxidation. A detailed description of the oxide crack mechanism is reported in (Neu and Sehitoglu, 1989a), (Neu and Sehitoglu, 1989b). There, the oxidation damage term is modeled as:

$$\frac{1}{N_f^{ox}} = \left[\frac{h_{cr}\delta_0}{B\Phi^{ox}K_p}\right]^{-1/\beta} \frac{2(\Delta\varepsilon_{mech})^{1+2/\beta}}{\dot{\varepsilon}_{mech}^{1-(a/\beta)}}, \tag{5}$$

where K_p is the parabolic oxidation parameter, which is a function of temperature; δ_0, h_{cr}, B and a are material constants, and ε_{mech} is the mechanical strain. The phasing factor Φ^{ox} is used as a sort of amplifier of the damage between phasings: it ranges from 0, which indicates that no oxidation damage results from the phasing, to 1, which indicates that the coupling of the environment and phasing is most detrimental to a component's life. Φ^{ox} is a function of the ratio of the thermal and the mechanical strain rates, and is equal to 1 for in-phase TMF, which is the case in a combustion chamber (when the load increases, also the temperature and the pressure increase).

In general, K_p is not constant for a cycle where temperature varies with time. Measurements of the oxide thickness development with time for Inconel 718 are provided in literature, for example in (Al-Hatab et al., 2011) and (Greene and Finfrock, 2000). Inconel 718 oxidation follows a typical parabolic growth law in the form $h_0 = \sqrt{K_p t}$, where h_0 is the oxide thickness and t is the time. The oxide thickness growth is sometimes measured in terms of weight gain per unit area:

$$\left(\frac{\Delta w}{A}\right) = \sqrt{K_p' t}, \tag{6}$$

where $\Delta w/A$ represents the weight gain per unit area. If its units are (mg/cm^2), then K_p' has the unit $mg^2/cm^4 s$. As reported in (Greene and Finfrock, 2000), one can assume that during oxidation of Inconel all oxides formed are monoatomic (i.e., CrO, NiO, and FeO), which would be the worst-case oxidation rate. In this case, the ratio of the mass of Inconel oxidized to the mass of oxygen gained due to oxidation would be 3.54. In other words, if the sample gained 1 g of mass during oxidation due to oxygen uptake, then 3.54 g of Inconel would have been oxidized. Using the Inconel density of 8.22 g/cm^3 and multiplying Eq. 6 by $(3.54)^2$, the average depth of penetration of the oxidation into the surface of the metal can then be calculated. Penetration depth estimates made by this procedure will result in maximum penetration estimates due to the conservative assumptions in the oxidation chemistry stoichiometry. In this way, it is possible to derive K_p from K_p', enabling to obtain the hard to measure h_0 from the experimental $\Delta w/A$. Values of K_p at high temperatures are reported in Tab. 1. In Fig. 1, the oxide layer growth curves for various temperatures are plotted against experimental data (Al-Hatab et al., 2011). A summary of the constants used in the prediction model is provided in Tab. 2. The data is taken from different sources.

3. Lifing assessment: procedure and tools

3.1. Computational Fluid Dynamics Simulations

The component examined in this analysis is an in-house modified combustion chamber of the MGT *Enertwin* from the dutch company *MTT* (Visser et al., 2010). This burner was entirely additive-manufactured with Inconel 718 and consists of six nozzles (see Fig. 2) injecting methane. Fully coupled, steady state, Conjugated Heat Transfer- (CHT)

Table 1: Parabolic oxidation constant as a function of temperature for Inconel 718 according to (Al-Hatab et al., 2011) and (Greene and Finfrock, 2000).

Temperature, K	K'_p, mg^2/cm^{4}s	K_p, μm^2/s
1023	6.75E-8	1.22E-6
1123	2.13E-7	3.95E-6
1173	2.67E-6	4.95E-5
1273	4.67E-5	8.66E-4
1373	9.60E-5	1.78E-3
1473	1.94E-4	3.60E-3
1573	2.42E-4	4.49E-3

Table 2: Oxidation damage material constants for Inconel 718 (Amaro et al., 2010), (Sehitoglu and Boismier, 1990).

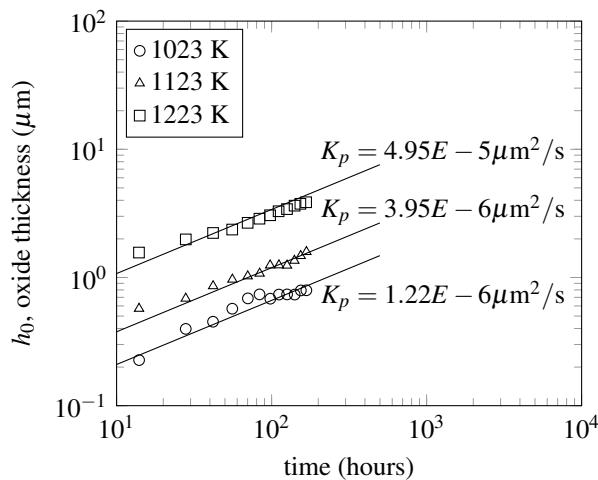| Constant	Value	Units
a	1.5	-
β	1.5	-
B	$6.93 \cdot 10^{-3}$	s$^{-0.5}$
δ_0	$1.12 \cdot 10^{-10}$	μm $\cdot$ s$^{-0.75}$
K_p	$f(T)$, see Tab. 1	μm^2/s
h_{cr}	461.4	μm
ξ^{ox}	0.44	-

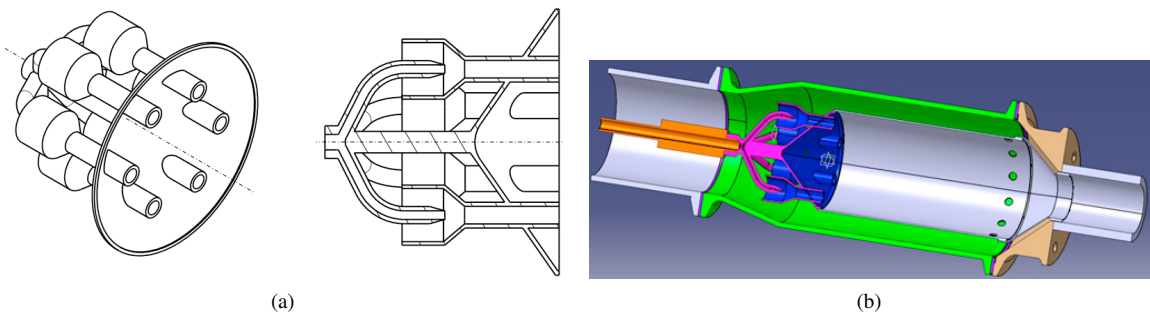Fig. 1: Oxide layer growth in time for Inconel 718 at various temperatures.

Fig. 2: Representation of the tested combustion chamber. Burner only (a) and complete combustion chamber (b).

CFD RANS simulations have been executed using the commercial software Ansys Fluent. The combustion mechanism for methane/air consists of a reduced subset of 22 species from the much larger reaction mechanism GRIMech 3.0 (Smith et al., 1999). Radiation heat transfer of the hot gases is included with the Discrete Order model.

Table 3: Steady state properties at various setting points. N = rotational speed, P_{th} = thermal power, P_{el} = electrical power, and P_f = fuel power.

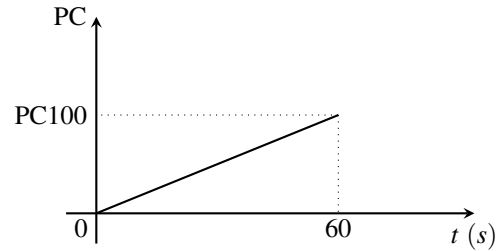| SP	N (krpm)	P_{th} (kW)	P_{el} (kW)	P_f (kW)
PC20	180	7.60	0.73	10.56
PC40	190	8.40	1.02	11.96
PC60	200	10.00	1.34	13.44
PC70	210	11.30	1.69	15.46
PC80	220	12.50	2.04	17.54
PC90	230	14.20	2.39	19.77
PC100	240	15.60	2.70	22.17

Fig. 3: Time over load point, representing a cold-start to full-load (1 minute).

Table 4: Elastic modulus, Poisson ratio and thermal expansion coefficient of Inconel 718 with different temperatures (Agazhanov et al., 2019), (Special Metals Corporation, 2007).

Temperature (°C)	Young's Modulus (MPa)	Poisson's Ratio (-)	α (10^{-6}/°C)
22	200000	0.294	-
100	196299	0.287	13.91
200	189981	0.279	14.59
300	184453	0.271	15.14
400	179320	0.271	15.64
500	172608	0.270	16.30
600	165895	0.275	18.29
700	156813	0.291	19.04
800	148126	0.316	26.21
900	133122	0.331	23.24
1000	120091	0.349	21.77
1100	98374	0.402	22.57

Table 5: Yield strength and tangent modulus of Inconel 718 with different temperatures (Mucci and Harris, 1976).

Temperature (°C)	Yield Strength (MPa)	Tangent Modulus (MPa)
20	1030	1000
400	1000	1000
500	980	500
650	860	500
750	760	500

A MGT MTT Enertwin was tested under various working conditions during experiments conducted at DLR, Stuttgart (Seliger-Ost et al., 2020), (Cirigliano et al., 2022). The whole system, including turbine, compressor, recuperator and generator, can run at partial-load down to 20% of the nominal power. The setting points are called Power Control (PC) and vary between PC100 (full-load) and PC20 (the minimum partial-load) with intervals of 10. Table 3 shows thermal, electrical and fuel power for different PCs. The Multiple load history considered in this analysis is a cold-start, i.e. passing from environmental conditions to full-load (PC100) over one minute (Fig. 3). Material properties of Inconel 718 (also called IN718, GH4169 or UNS N07718 superalloy) are reported in Tab. 4 and 5.
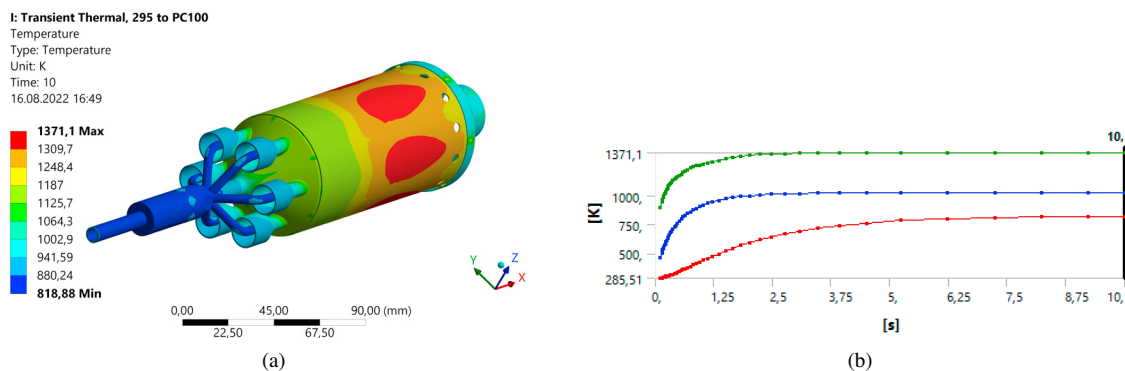
Fig. 4: Temperature distribution (left) of the combustion chamber structure at full-load (PC100) and temperature-transient over 60 seconds (right).

3.2. User Programmable Feature USERMAT in ANSYS

User Programmable Features (UPFs) are a highly effective and flexible tool to tailor the behavior of the Ansys APDL program to suit individual requirements. This is performed by writing a custom subroutine in the C, C++, or Fortran programming languages. One of such subroutines is USERMAT, which is particularly used to define non-linear stress-strain relationships and custom damage evolution laws, like in this study. In this section, the implementation of a damage-based material model via a UPF is outlined.

USERMAT subroutine is called at every time iteration and executed on each element of the computational grid. The input parameters, such as loads and temperature, are defined by the user during the modeling step. Current stresses, strains and strain increments are the inputs at the start of the timestep. At each iteration, a new elastic, plastic, and thermal strain, an effective Young's modulus and damage evolution are computed based on the constitutive equations and material model described in the previous sections. USERMAT then updates the stresses and the material Jacobian matrix and these values are sent back to the main Finite Element code as outputs (Lin, 1999). The status of every element is checked at every time increment using a strength lifetime failure criterion: when the maximum damage of the structure reaches a threshold value, the subroutine is stopped and the present time is recorded as the lifetime of the component.

4. Results

The fully coupled CHT-CFD simulations provide the spacial distribution of temperature, pressure and heat transfer coefficients for every operative point PC. Figure 4a shows the temperature distribution over the combustion chamber for the PC100, and Fig. 4b shows the thermal-transient over the cold-start. It can be seen that a steady state is obtained approximately within the first 10 seconds. The highest temperatures are located in the second half of the combustion chamber, as expected, due to the high convection and radiation caused by the flame.

The temperature distribution in space and time can be then fed as input in a structural analysis in Ansys Mechanical, where principal stresses and strains are generated for this load history. The combustion chamber life is then assessed using the Neu-Sehitoghlu TMF model implemented via the UPF USERMAT. Figures 5a, 5b, 5c and 5d show the equivalent stress, plastic strain, creep strain and oxidation damage after 60 seconds from the start, respectively. It can be seen that the area presenting the highest stresses and strains is the junction between the combustion flame tube and the exit cone, even though the highest temperatures are located elsewhere. This is due to the fact that this small segment is connecting two much larger components. Geometrical non-linearities cause high mechanical strains, which in turn promote stress concentration. High temperatures also promote larger K_p, which induce a more pronounced oxidation (see Eq. 5). The oxide damage D^{ox} is in the order of 10^{-12}, and the creep damage D^{creep} is negligible for such a short time. Creep would most likely assume a major role for much longer operations, in the order of hours. The scope of this analysis was to implement the complex TMF in Ansys mechanical through a UPF USERMAT, and this has been

(a) *Equivalent Stress*

(b) *Plastic Strain*

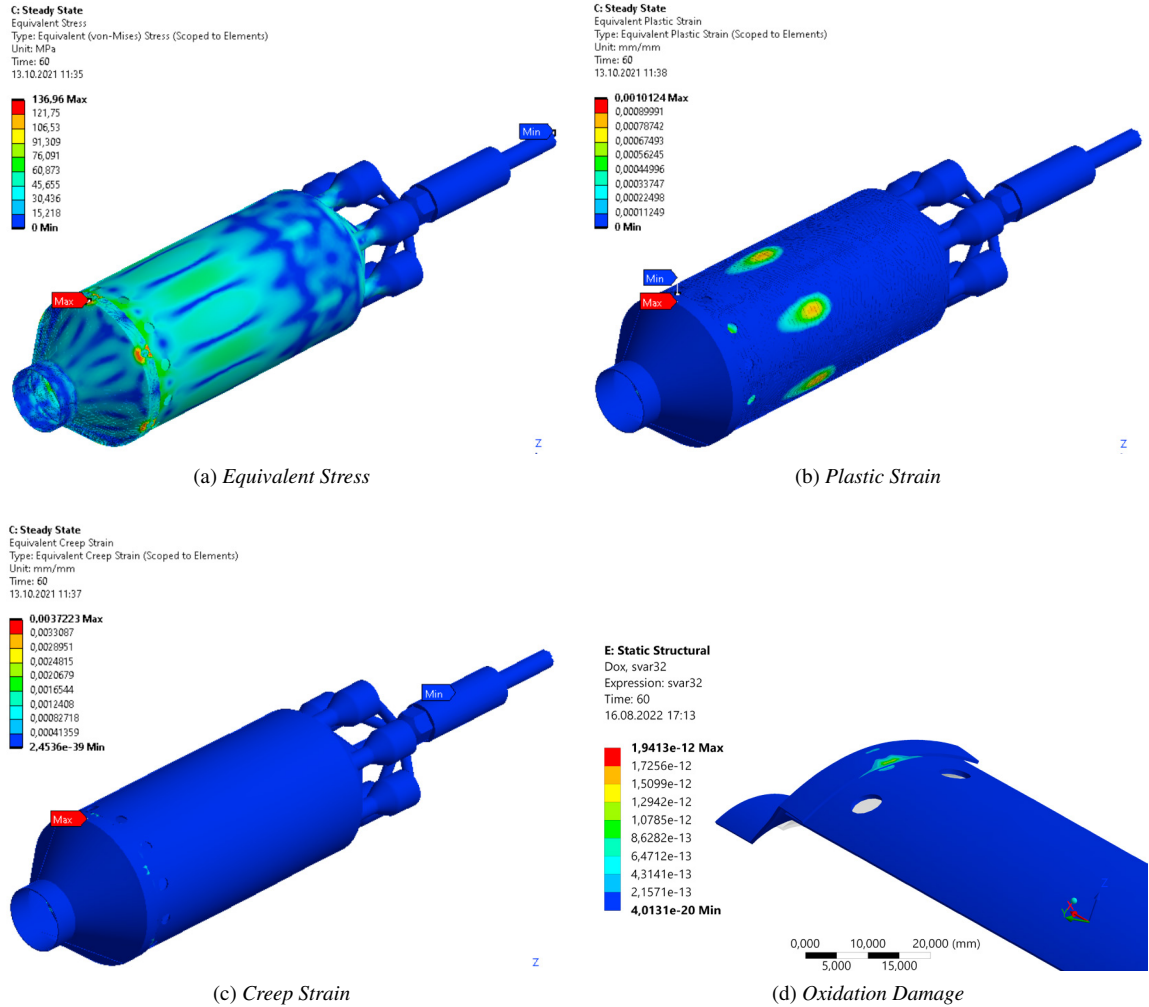(c) *Creep Strain*

(d) *Oxidation Damage*

Fig. 5: Distribution of variables of interest in the combustion chamber after 60 seconds from start (PC100).

successfully done. Longer simulations, such as operation at steady state for several hours, will be performed in future works, and lifing will be provided for those real operative profiles.

5. Conclusions

TMF behavior and lifetime prediction of a MGT combustion chamber made of Inconel 718 superalloy were investigated in realistic temperature range and operative conditions. Numerical simulations have been performed by implementing the Neu-Sehitoglu model in Ansys Mechanical using a UPF. It was assumed that fatigue plays a minor role compared to creep and oxidation, since no mechanical forces were directly applied on the structure. The following conclusions can be drawn:

- The junctures between components, such as contacts and weldings, present stress concentration due to geometrical non-linearities. There, plasticity, creep and oxidation damage may occur.
- To be monitored are also the zones at highest temperature, close to the flame, where creep plays a major role.

- Due to lack of experimental data, these conclusions assume a qualitative significance only (i.e. location of the damage but not its amount), and should be supported by investigation of components at end-life. If, after measurements, the most damaged zones (e.g. affected by cracks) would coincide with those mentioned above, this analysis would be a valid and powerful tool for the design and the maintenance of MGT combustion chambers.

References

Abu, A.O., Eshati, S., Laskaridis, P., Singh, R., 2014. Aero-engine turbine blade life assessment using the neu/sehitoglu damage model. International Journal of Fatigue 61, 160–169.

Agazhanov, A.S., Samoshkin, D.A., Kozlovskii, Y.M., 2019. Thermophysical properties of inconel 718 alloy. Journal of Physics: Conference Series 1382, 012175. URL: https://doi.org/10.1088/1742-6596/1382/1/012175, doi:10.1088/1742-6596/1382/1/012175.

Al-Hatab, K.A., Al-Bukhaiti, M., Krupp, U., Kantehm, M., 2011. Cyclic oxidation behavior of in 718 superalloy in air at high temperatures. Oxidation of metals 75, 209–228.

Amaro, R.L., Antolovich, S.D., Neu, R.W., Staroselsky, A., 2010. On thermo-mechanical fatigue in single crystal ni-base superalloys. Procedia Engineering 2, 815–824.

Cirigliano, D., Grimm, F., Kutne, P., Aigner, M., 2022. Economic analysis and optimal control strategy of micro gas-turbine with batteries and water tank: German case study. Applied Sciences 12. URL: https://www.mdpi.com/2076-3417/12/12/6069, doi:10.3390/app12126069.

Greene, G., Finfrock, C., 2000. Oxidation Of Inconel 718 In Air At Temperatures From 973K To 1620K. Technical Report. Brookhaven National Lab.(BNL), Upton, NY (United States). doi:https://doi.org/10.2172/777719.

Halfpenny, A., Anderson, R., Lin, X., 2015. Isothermal and thermo-mechanical fatigue of automotive components. SAE Technical Paper doi:https://doi.org/10.4271/2015-01-0548.

Harrison, G., Tranter, P., Williams, S., 1996. Modelling of thermomechanical fatigue in aero engine turbine blades. ROLLS ROYCE PLC-REPORT-PNR .

Lemaitre, J., 1985. A continuous damage mechanics model for ductile fracture .

Lin, G., 1999. Ansys user material subroutine usermat. ANSYS, Canonsburg, PA .

Miner, M.A., 1945. Cumulative damage in fatigue. American Society of Mechanical Engineers .

Mucci, J., Harris, J.A.S., 1976. Influence of gaseous hydrogen on mechanical properties of high temperature alloys, in: Pratt & Whitney Aircraft Group (Ed.), Aerospace Structural Metal Handbook. Handbook Operations, Purdue University. volume 4, p. 34.

Neu, R., Sehitoglu, H., 1989a. Thermomechanical fatigue, oxidation, and creep: Part i. damage mechanisms. Metallurgical transactions A 20, 1755–1767.

Neu, R., Sehitoglu, H., 1989b. Thermomechanical fatigue, oxidation, and creep: Part ii. life prediction. Metallurgical transactions A 20, 1769–1783.

Sehitoglu, H., Boismier, D., 1990. Thermo-mechanical fatigue of mar-m247: Part 2—life prediction. Transactions of the ASME .

Seliger-Ost, H., Kutne, P., Zanger, J., Aigner, M., 2020. Experimental investigation of the impact of biogas on a 3 kw micro gas turbine flox®-based combustor. Turbo Expo: Power for Land, Sea, and Air Volume 4B: Combustion, Fuels, and Emissions. URL: https://doi.org/10.1115/GT2020-15556, doi:10.1115/GT2020-15556.

Smith, G.P., Golden, D.M., Frenklach, M., Moriarty, N.W., Eiteneer, B., Goldenberg, M., Bowman, C.T., Hanson, R.K., Song, S., Gardiner, W.C.J., Vitali, V.L., Qin, Z., 1999. The gri-mech 3.0 URL: http://www.me.berkeley.edu/gri_mech/.

Special Metals Corporation, 2007. Special metals datasheet. Publication Number SMC-045 URL: https://www.specialmetals.com/documents/technical-bulletins/inconel/inconel-alloy-718.pdf.

Visser, W.P.J., Shakariyants, S.A., Oostveen, M., 2010. Development of a 3 kW microturbine for CHP applications. Journal of Engineering for Gas Turbines and Power 133. URL: https://doi.org/10.1115/1.4002156, doi:10.1115/1.4002156.

Zhang, L., 1995. Research of fatigue failure on high-temperature parts based on damage mechanics. Ph.D. thesis. Beijing University of Aeronautics and Astronautics.